INSTITUTE OF PHYSICS PUBLISHING NANOTECHNOLOGY
Nanotechnology **17** (2006) 3071–3080 doi:10.1088/0957-4484/17/12/043

Stability of dynamic force microscopy with the self-oscillator method

M Labardi

JILA, University of Colorado and NIST, Boulder, CO 80309-0440, USA
and
PolyLab CNR-INFM, Largo Bruno Pontecorvo 3, 56127 Pisa, Italy

E-mail: labardi@df.unipi.it

Received 3 February 2006, in final form 19 April 2006
Published 2 June 2006
Online at stacks.iop.org/Nano/17/3071

Abstract
Dynamic force microscopy (DFM) with the self-oscillator (SO) method is not generally subjected to the instability effects typical of tapping-mode DFM, as confirmed experimentally. The inherent stability of SO-DFM is related to phase locking of the cantilever oscillation to the excitation signal. Such phase locking determines univocally the oscillation state (i.e. amplitude and frequency) on the resonance curve, even when multiple amplitude values are compatible with a given frequency. By modelling the behaviour of an air-operated DFM system, it is found that, while stabilizing tip/surface distance for DFM imaging at constant frequency shift, and beyond a certain critical phase value, instabilities are possible in the SO constant-excitation amplitude mode. However, such instabilities cannot affect dynamic force spectroscopy approach curves, because of phase locking. By extension to vacuum operation, this result can confirm the origin of jumps in frequency shift found on some experimental DFM approach curves, for instance between non-passivated silicon tips to specific surface atomic sites of reconstructed silicon, since instrumental effects of the SO method can be ruled out.

1. Introduction

Dynamic force microscopy (DFM) in the self-oscillator (SO) method [1] has a relevant role as an atomic-scale surface imaging and spectroscopic tool. In spite of a rather complicated experimental implementation compared to the simpler low-amplitude non-contact [2] and high-amplitude tapping-mode DFM [3], SO-DFM provides higher measurement bandwidth for imaging [1] and more straightforward interpretation of approach curves for dynamic force spectroscopy [4, 5]. Furthermore, instability effects typical of tapping-mode DFM [6] are not observed experimentally with the SO method, although anticipated by some theoretical studies [7]. In this paper it is shown that SO-DFM is characterized by inherently high stability, which can be evinced by the analysis of the DFM cantilever motion when properly taking into account the phase-locking condition that is the essential feature of the SO method.

Understanding possible instability effects in the SO method is important for clarifying the physical mechanisms responsible for the observed jumps in the frequency shift signal during the approach of a DFM tip to specific atomic sites by using the constant-excitation amplitude (CE) SO method [8], as observed in experiments [9, 10]. In [10] it was found that jumps in frequency shift during the approach of a silicon tip were recorded at specific lattice sites of a Si(111) 7 × 7 reconstructed surface. The jumps were present depending on the type of atomic site to which the tip was approached, and were not present when using a passivated Si probe. Therefore, DFM approach curves were demonstrated to provide lattice-site selectivity. A model of covalent bonding formation between dangling bonds on the Si tip and the surface has been proposed to explain such discontinuities [10]. A similar behaviour was reproduced by *ab initio* simulations between Si and InAs [11]. In general, such jumps can be obtained by introducing a hysteretic potential, which simulates a dissipative bonding formation and breaking phenomenon [12]. However, the model of covalent bond formation awaits stronger confirmation, for instance by checking that dynamic force spectroscopy in the CE-SO mode is not subjected to instabilities that could generate such jumps as measurement artefacts. In the present paper, such a demonstration is provided, thereby strengthening the

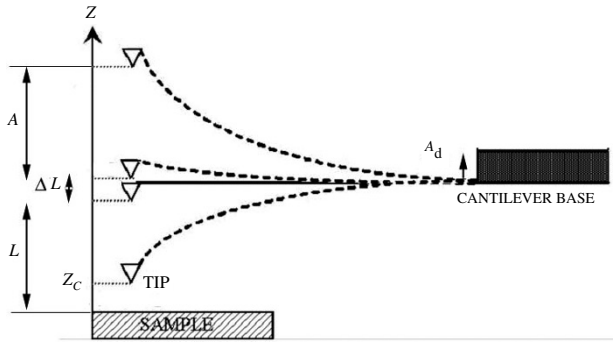

Figure 1. Sketch of the oscillating probe/cantilever system.

above-mentioned model, and more generally describing the instabilities that can be observed by using SO-DFM, with special attention to the CE mode for which discontinuities in the approach curves have been observed experimentally. An air-operating DFM has been considered in this analysis, but there is no hindrance to extending it also to vacuum-operated systems.

2. Model

Let us consider a standard dynamic force microscope setup, comprising a tip mounted on a cantilever and facing a sample surface (figure 1). Tip–sample separation can be varied, with L being the separation between their supports. The physical distance between the apex atoms of the tip and the local sample surface is indicated by z. In static-mode force spectroscopy, these quantities are slowly varying. In DFM instead, surface forces are sensed by detecting amplitude and frequency perturbations to the nearly sinusoidal motion of the tip vibrating perpendicularly to the surface. As the cantilever deflection has a periodic oscillation, z oscillates as $z(t) = L + \delta(t)$, where δ indicates the cantilever deflection, and we define $L = 0$ as the separation corresponding to $z = 0$ with an undeflected cantilever ($\delta = 0$). Using DFM to diagnose surface forces is not straightforward, and deconvolution procedures are required in order to obtain the local tip/sample interaction potential $F_{\rm cons}(z)$ from the measured 'approach curves' of frequency shift and oscillation amplitude versus L. For this purpose, procedures for both constant amplitude (CA) [4] and CE [5] spectroscopy modes have been developed. The equivalence of the two modes for spectroscopic applications has also recently been checked experimentally [13]. Our aim is instead to analyse general features of SO operation and stability; therefore, simple model potentials will be assumed, and a theoretical analysis will be carried out to describe the features of approach and lever-resonance curves that are relevant to the study of DFM instability.

Let us briefly recall the working principle of a typical DFM. The cantilever is made to oscillate by means of a mechanical excitation, usually induced by a dithering piezoslab. In non-contact and tapping-mode DFM, the dithering amplitude $A_{\rm d}$ and its frequency f are fixed at (or near) the resonance of the cantilever. The surface interaction produces changes in the oscillation amplitude A as well as in its phase difference ϕ compared to the dithering. In particular, phase imaging [14] provides information on the surface composition, by measuring the energy dissipation occurring at the intermittent contact [15]. SO-DFM operates instead by means of a self-oscillation, induced by a suitable amplifier that loops the dithering signal (driving the piezoslab) with the detected cantilever position [1], so that the oscillation phase ϕ must be a constant, as described below. The self-oscillation can be realized either at fixed A, in the CA mode, or at fixed $A_{\rm d}$, in the CE mode, by means of an automatic gain control (AGC) [1]. Therefore, both f and $A_{\rm d}$ are allowed to vary in CA mode, while both f and A can vary in CE mode.

In a previous publication [16], the description of a SO-method DFM was given, by carrying out expressions for the frequency shift $\Delta f = f - f_0$ with respect to the unperturbed oscillation at f_0, and the phase ϕ. Such quantities are functions of L, A, $A_{\rm d}$, the resonant frequency $f_{\rm r}$, depending on the conservative tip/surface interaction $F_{\rm cons}(z)$, and the effective quality factor $Q_{\rm eff}$, which takes into account the dissipation $P_{\rm surf}$ taking place between the tip and surface due to a dissipative force $F_{\rm diss}(z, {\rm d}z/{\rm d}t)$. The analysis was therefore restricted to the case of small frequency shift ($\Delta f \ll f_0$) in order to obtain simplified relations in which the essential physics was still contained. The exact solution of the equation of motion obtained by Fourier analysis with the ansatz $z(t) = A\cos(\omega t - \phi) + \text{constant}$, where $\omega = 2\pi f$, gives for the phase:

$$\sin^2\phi(A, L) = \left(\frac{A}{A_{\rm d} Q_{\rm eff}(A, L)}\right)^2, \qquad (1)$$

which is the same also in the approximated case, while the expression of f results:

$$f(A, L) = f_0 \sqrt{\frac{f_{\rm r}(A, L)}{f_0} \pm \sqrt{\left(\frac{A_{\rm d}}{A}\right)^2 - \frac{1}{Q^2_{\rm eff}(A, L)}}}. \qquad (2)$$

The $\pm$ signs indicate opposite branches of the resonance curve ($\phi > \pi/2$ and $<\pi/2$, respectively). $f_{\rm r}(A, L)$ is the *resonance frequency*, with $\phi = \pi/2$ and maximum oscillation amplitude, while $Q_{\rm eff}(A, L)$ is the *effective quality factor* that takes into account surface dissipation. In the approximated case we have (equation (5) of [16]):

$$f(A, L) \approx f_{\rm r}(A, L) \pm \frac{f_0}{2}\sqrt{\left(\frac{A_{\rm d}}{A}\right)^2 - \frac{1}{Q^2_{\rm eff}(A, L)}}. \qquad (3)$$

The actual lever motion with surface interaction may differ slightly from $A\cos(\omega t)$ by presenting higher harmonic components. Such modes should be taken into account for the accurate determination of internal energy dissipation [17]; however, for our analysis we will calculate the effects of $F_{\rm cons}$ and $F_{\rm diss}$ only on the fundamental-mode component of motion in the steady state, in order to compare to most of the previous literature, which follows the same approximation.

The resonance frequency is defined as $f_{\rm r}(A, L) = f_0(1 - F_{1,\rm cons}/kA)^{1/2}$, where $F_{1,\rm cons} = (\omega/\pi)\int F_{\rm cons}(z(t))\cos(\omega t)\,{\rm d}t$. The approximated result of [16] was $f_{\rm r}(A, L) \approx f_0(1 - F_{1,\rm cons}/2kA)$, which is valid for small frequency shift. The effective quality factor is defined as $Q_{\rm eff} = 1/(1/Q + F_{1,\rm diss}/fkA)$, with $F_{1,\rm diss} = (\omega/\pi)\int F_{\rm diss}(z(t), {\rm d}z(t)/{\rm d}t)$

$\sin(\omega t)\,\mathrm{d}t$. We make explicit the dependence on separation of the function r, defined as in [7]:

$$r(A, L) = \frac{1}{\pi k A^2} \int_0^{\frac{2\pi}{\omega}} F_{\mathrm{cons}}(z + L) A \cos(\omega t - \phi)\, \mathrm{d}(\omega t). \tag{4}$$

Therefore, the term $r(A, L)$ corresponds here to $(1 - f_\mathrm{r}^2/f_0^2)$, or to $-2(f_\mathrm{r} - f_0)/f_0$ in the approximated case. This formulation is equivalent to those of Giessibl [18] and Durig [19], which have general validity provided that $|F_{\mathrm{cons}}(z_\mathrm{c})| \ll kA$, where $z_\mathrm{c} = L - A$ is the closest approach distance reached by the tip during its oscillation. Such a condition is generally satisfied for small frequency shifts. Equation (2) (and equation (3) for small Δf) is essentially the generalization of equation (4) of [7] including dissipative forces.

The definition of $z_\mathrm{c} = L - A$ should be corrected by a term $\Delta L = A\Delta f/f_0$ [16], although this is not generally recognized. This term stems from the 0th order of the Fourier decomposition of the interaction force, and might be of importance for the proper study of sub-nanometre range interactions, since it implies the recalibration of the distance axis z_c. However, for small frequency shifts the approximated expression will be used, since the correction ΔL is negligibly small and its inclusion would excessively complicate our analytical treatment.

Both f_r and Q_eff will be calculated by assuming a realistic model form of the conservative and dissipative interactions. For a spherical probe tip of radius a and $z < a$, the van der Waals force is $-C_2/z^2 = -(A_\mathrm{H}/2\pi)(a/z^2)$. Using $A_\mathrm{H} = 2 \times 10^{-19}$ J as the Hamaker constant for a Si probe and sample, to match the experimental data of [16] we will use $C_2 = 10$ nN nm^2, which corresponds to a tip radius of about 30 nm. We add a repulsive component C_6/z^6 that yields a $\Delta f_\mathrm{r}(z_\mathrm{c})$ that resembles that measured in the repulsive region in [16], and a minimum at $z_\mathrm{c} = 1.2$ nm similar to such data. Thus $F_{\mathrm{cons}}(z) = -C_2/z^2 + C_6/z^6$, with $C_6 = 100$ nN nm^6. The expression here used for $F_{\mathrm{cons}}(z)$ was chosen instead of the Morse potential used in [16], because it resulted in more stable numerical solution of equations (1) and (2), which will be necessary for the forthcoming analysis. The two potential forms are very similar, and the qualitative effects investigated here appear to have no particular dependence on the details of the potential itself.

From [18], this F_{cons} yields a resonance shift of:

$$f_\mathrm{r}(z_\mathrm{c}, A) - f_0 = f_0 \frac{(-C_2 I(2) z_\mathrm{c}^{-3/2} + C_6 I(6) z_\mathrm{c}^{-11/2})}{\sqrt{2}\pi k A^{3/2}}, \tag{5}$$

where $I(2)/\pi = 0.5$, and $I(6)/\pi = 0.25$. This expression is valid only for high oscillation amplitudes ($A \gg z_\mathrm{c}$), while in the general case the frequency shift should be carried out from equation (2).

For F_{diss}, we follow [20] in choosing a dissipative force that is an exponential times the probe velocity,

$$F_{\mathrm{diss}}\left(z, \frac{\mathrm{d}z}{\mathrm{d}t}\right) = \frac{\mathrm{d}z}{\mathrm{d}t} \Gamma \mathrm{e}^{-\frac{z}{\sigma}}, \tag{6}$$

which, in the case of oscillatory motion with amplitude A and closest approach z_c, yields $F_{\mathrm{diss}}(z, z_\mathrm{c}, A) \approx -2\pi\Gamma f(z_\mathrm{c}, A)[2A(z - z_\mathrm{c})]^{1/2} \exp(-z/\sigma)$. The surface-induced power dissipation P_{surf} results from the integration of F_{diss} over one oscillation period:

$$P_{\mathrm{surf}}(z_\mathrm{c}, A) \approx (2\pi\sigma)^{3/2} A^{1/2} f(z_\mathrm{c}, A) \Gamma \mathrm{e}^{-\frac{z_\mathrm{c}}{\sigma}}. \tag{7}$$

These expressions for $F_{\mathrm{diss}}(z, z_\mathrm{c}, A)$ and $P_{\mathrm{surf}}(z_\mathrm{c}, A)$ are given in the approximation $A \gg \sigma$, whereas for smaller oscillation amplitudes the analytical solution becomes more complicated [20]. Again, to retain a resemblance to the data of [16], we take $\sigma = 0.6$ nm to represent the dissipative force. The resulting Q_eff, related to $P_{\mathrm{surf}}(z_\mathrm{c}, A)$ as [16]

$$\frac{1}{Q_\mathrm{eff}(z_\mathrm{c}, A)} = \frac{1}{Q} + \frac{\pi P_{\mathrm{surf}}(z_\mathrm{c}, A)}{kA^2}, \tag{8}$$

therefore has an explicit dependence on frequency shift, which can be neglected only if we approximate $f(z_\mathrm{c}, A) \approx f_0$, hence for small frequency shifts. In order not to complicate the analysis, we will make such assumption. The chosen potential forms are rather general and commonly used in literature [4, 5]. Let us note that for vacuum operation, where Q becomes much higher, surface dissipation becomes even more important for the behaviour of the system. Here we choose to treat the air-operation case only, but there is no hindrance to applying the same conclusions to vacuum operation.

The evolution of the cantilever resonance curve by changing the separation L provides a clear illustration of the behaviour of a DFM system during the performance of an approach curve. When the tip is far enough from the sample, no interaction occurs and the resonance curve has a Lorentzian lineshape. By decreasing L, the nonlinear interaction terms deform the Lorentzian, giving rise to a typical needle-like lineshape (see e.g. [7, 16]) characterized by a multivalued character, i.e. multiple solutions $A(f)$ for a given range of frequencies. Dissipative terms in the interaction can inhibit the appearance of such a needle-like feature. Figure 2 shows

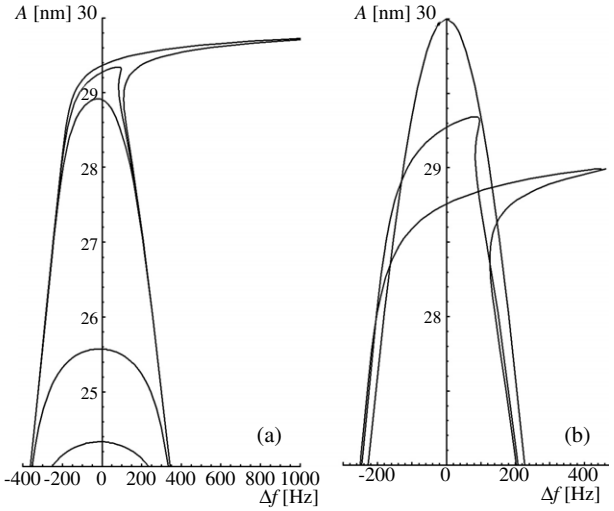

Figure 2. (a) Resonance curves at fixed separation ($L = A_0 + \sigma$, with $A_0 = 30$ nm, $\sigma = 0.6$ nm) for different dissipation coefficients (in order of decreasing peak amplitude): $\Gamma = 0$, 3×10^{-8}, 10^{-7}, 10^{-4} and 10^{-3} kg s^{-1}. (b) Resonance curves at different separations ($L = A_0 + 150\sigma$, $A_0 + \sigma$, A_0) in the dissipative case, for $\Gamma = 3 \times 10^{-8}$ kg s^{-1}.

resonance curves that we used to describe the behaviour of a DFM in both tapping mode and CE-SO mode. In figure 2(a), the top of a resonance curve is shown (versus fixed separation $L = A_0 + \sigma$, in this case $L = 30.6$ nm with $A_0 = 30$ nm) in the case of no dissipation (a needle-like structure) as well as of four different friction coefficients within $F_{\rm diss}$ ($\Gamma = 3 \times 10^{-8}, 10^{-7}, 10^{-4}$ and 10^{-3} kg s^{-1}). Thus, with increasing dissipation, eventually the multivalued curve disappears. The parameters used, maintained for all the forthcoming calculations unless otherwise specified, are the following: cantilever spring constant $k = 50$ N m^{-1}; free resonance frequency $f_0 = 263\,315$ Hz; free quality factor $Q = 280$; free oscillation amplitude $A_0 = 30$ nm, which match with those of [16], and refer to air operation.

Figure 2(b) illustrates the evolution of the resonance curve as a function of the separation, in the presence of a dissipative term. The amplitude decreases with L, which would not be possible without surface dissipation, from simple arguments of energy conservation. In the case of low dissipation that is shown ($\Gamma = 3 \times 10^{-8}$ kg s^{-1}), a needle-like structure is still present. The behaviour of a tapping-mode DFM can be analysed by tracing an $f =$ constant line on this plot and by following the interceptions of such a line with the resonance curve while L is changed. It is evident that three solutions exist for a range of positive frequency shifts, and since in tapping mode the oscillation phase is free to vary, each of such states can be sustained by the oscillator; when the tip/sample interaction deforms the resonance curve in such a way to eliminate one of the possible states, a jump in amplitude (and phase) will occur if the system was oscillating in such a state, otherwise no jumps will occur. Therefore, the actual state of the system will be determined by its previous history, namely on how L was varied before (whether increased or decreased). This illustrates the hysteresis behaviour observed in tapping-mode approach curves, although alternate descriptions of the same phenomenon can be given [6].

In the case of the self-oscillator method, the oscillator loop is subjected to the Barkhausen criterion [21] which constraints the loop phase and gain to be a constant. In particular, the overall loop phase must be null, therefore the phase of the oscillating probe/cantilever system must match that of the self-oscillator amplifier, which is an adjustable constant independent of the operating frequency. This locks the cantilever oscillation phase to a constant value that can be set by the user by adding a phase shifter into the oscillator loop. It is evident that, for each L value and consequently for each resonance curve obtained, the cantilever will oscillate at the frequency and amplitude compatible with such a phase. The value of A is carried out as the solution of equation (1) with $\phi = \phi_{\rm set}$ at a given L. The separation $L(A)$ can be obtained analytically in the case of the force $F_{\rm cons}(z)$ used to calculate equation (5), with an explicit phase dependence, therefore it could be used to obtain $f(A, \phi)$ in this analysis. However, a numerical solution may be necessary in general. Afterwards, the corresponding value of f is calculated by means of equation (2). To visualize the evolution of the oscillation state on the resonance plot, one should trace an *isophase curve*, in place of the simple $f =$ constant line used for the tapping mode. Such a curve is comprised of all the oscillation states compatible with a fixed phase value. Figure 3 shows an example of isophase curves plotted together with the free resonance curve. A number of isophase curves are plotted, corresponding to $\phi = \pi/2$ and to several different phase values ($>\pi/2$ in the case shown) representative of different situations as regards the instability phenomenon (see section 4). If phase is $\pi/2$, the cantilever will oscillate at resonance (maximum oscillation amplitude). Phase values $<\pi/2$ characterize the branch of the resonance curve towards lower frequencies, while phase values $>\pi/2$ concern the higher-frequency branch. In general, each set phase value univocally determines an oscillation state (A, f) on the resonance curve, as seen by equations (1) and (2). This phenomenon (*phase locking*) happens even in the presence of surface dissipation (when $Q_{\rm eff} < Q$).

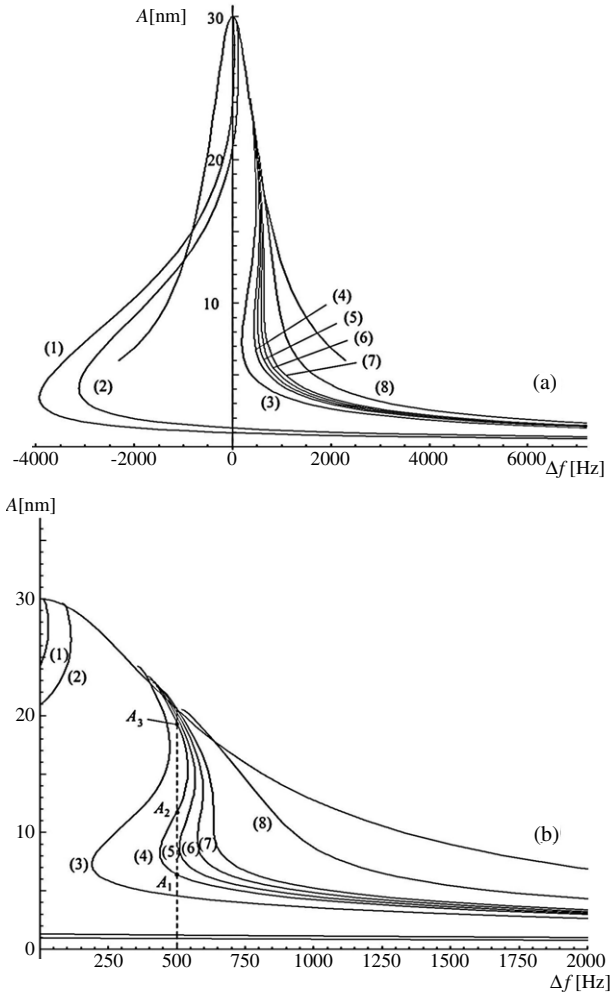

Figure 3. Isophase curves (a) and zoomed plot in the triple intersection region (b), for $\Gamma = 10^{-4}$ kg s^{-1} and the following phase values: (1) $\pi/2$; (2) $1.1\pi/2$; (3) $1.4\pi/2$; (4) $1.43\pi/2$; (5) $1.44\pi/2$; (6) $1.45\pi/2$; (7) $1.4608\pi/2 = \phi_{\rm c}$; and (8) $1.52\pi/2$. The resonance curve for large separation is also drawn.

3. Phase locking

Phase locking characterizes the self-oscillator method just like 'frequency locking' (i.e. fixed frequency operation) characterizes the tapping mode. In other words, in the SO

method, frequency is free to vary and phase is fixed, while in the tapping mode, phase is free to change and frequency is fixed. Phase locking is inherent in the SO method and is effective regardless of the operation mode that is adopted; namely, it is not limited to the CE mode, but also holds in the CA mode. It is worth noting that the same study here performed for the CE mode could be conducted as well for the CA mode, by replotting the resonance curves in the A_d versus f plane, or better, to retain similarity with the analysis of the CE mode, on the $1/G$ versus f plane, where $G = A_d/A$ is the self-oscillator amplifier gain determined by virtue of the Barkhausen criterion. Then, the isophase curves should be calculated by imposing constant A instead of constant A_d in equations (1) and (2). Such calculations for the CA mode have not been carried out yet, but even higher stability of this mode is expected in comparison to the CE mode, based on the experimental fact that no frequency shift jumps have been observed in approach curves recorded in CA mode. To compare with available experimental data in CE mode, only CE behaviour is investigated in this work; the study of CA mode, as well as of the high-Q case (vacuum operation) and of the contribution of higher-order harmonic vibration modes, will be the subject of further work.

The existence of phase locking reconciles discrepancies between theoretical predictions of artefacts in approach curves due to possible instabilities in the SO method with the experimental observations that instead evidence no such effect. Gauthier and Tsukada [7] anticipated an instability effect based on the fact that the needle-like resonance curve of a DFM cantilever presents multiple states with the same f but different amplitudes. However, such an effect was never observed experimentally. In [7] it is indeed assumed that the self-oscillator will oscillate at the highest amplitude compatible with the stable solution of the equation of motion. Actually, though, this cannot be realized using the SO method, since a fixed phase value is imposed by the SO itself. Therefore, the assumption made is not compatible with the actual behaviour of the SO. In particular, no switching between different states pertaining to the same resonance curve is possible, since different phase values pertain to each of those states (A, f). In a number of subsequent papers [22–24], an explanation of the high stability found experimentally with the SO method is attempted by means of transient effects during lateral scanning. If that was the case, however, the instabilities described in [7] could be observed at least in the case of very slow (or null) scanning speed, as well as while recording adiabatically slow approach curves. Furthermore, dynamic effects on the scan imply that images recorded by scanning in opposite directions should be different. Instead, such instabilities, as well as such asymmetries, were never observed, and the reason is that the phase locking of the SO method inhibits jumps between points of the same resonance curve with different phase, thereby 'stabilizing' the system. Therefore, it would have been enough to introduce the fundamental argument of phase locking to rule out the possibility of such an instability.

A comment by Hölscher *et al* [25] tried to explain the unsuccessful predictions of [7] by specifying that an equation of motion with a delayed time t_0 gives a more appropriate description of the oscillatory states obtained with the SO method compared to the equation of motion used in [7], by considering that, in the SO mode, the oscillator is self-driven by the feedback amplifier. We note, however, that equation (1) solved in [7] is not necessarily ascribed to a system externally driven by a sinusoidal driving force, as stated in [25]. Rather, it is the equation of motion of an oscillating system, used to carry out its mechanical behaviour (resonance curve), that is, the amplitude and phase pertinent to a given frequency. The solution of such an equation describes the physical properties of the system and is independent of how the oscillation is excited, either at constant frequency or by the SO method (constant phase). Instead, equation (1) of [25], derived from the previous analysis of [4], is solved with the ansatz $z(t) = A\cos(\omega t)$, while a phase lag is introduced by time-delaying the excitation term as $z(t - t_0)$, which imposes a phase lag $\phi_0 = 2\pi f t_0$ to the oscillator. No fixed phase is imposed instead in solving equation (1) of [7], but if we set $\phi = \phi_0$ in the solution, we must obtain the same result. There can be no difference between the solutions of equation (1) of [25] and equation (1) of [7] when $\phi = 2\pi f t_0$, since the equations become formally identical. Only, in equation (1) of [7] the frequency is given and the amplitude and phase are found, while in equation (1) of [25] the time delay is given and the frequency and amplitude are found. Therefore, by solving both equations in the full frequency (or time delay) range, the same resonance curve should be obtained. However, when f becomes different from the resonant frequency, the time delay t_0 does not correspond to a fixed phase term, but instead it gives a phase term that changes linearly with frequency. This corresponds to the behaviour of the self-oscillator circuit designed to have a fixed time delay, but not to the one designed to have a fixed phase shift, independent of frequency, which however is often found in the literature [1, 8, 16, 23, 24]. Thus, in such cases the solution of the time-delayed equation of motion does not correspond to the physical system realized in practice, that is, to a *phase-locked* system. Probably, the deviations from the actual physical behaviour, obtained by using equation (1) of [25], could be negligible for small frequency shift. However, the system is better described by equation (1) of [7], where a rigorously constant phase can be imposed. In any case, there is no need to introduce the time-delayed equation of motion just to explain the stability of the SO method, since it is enough to assume a constant phase in the solution of equation (1) of [7] to explain such stability: this corresponds to assuming phase locking of the self-oscillator.

4. Analysis

By analysing the trend of the isophase curves at different phase values, possible instabilities affecting the SO method in the constant-excitation amplitude mode can be evidenced. Consequently, it is worth investigating whether their occurrence could explain the jumps in frequency shift that are sometimes observed in the CE mode approach curves [9, 10]. To provide a thorough view of the problem, our analysis includes both imaging and spectroscopic modes of DFM in the CE-SO mode. For imaging purposes, it is possible to use either the oscillation amplitude stabilization [26] (case (i)) or the frequency shift stabilization [1] (case (ii)) to provide the topographic image of the surface by adjusting the separation L, by tracing contours of equal dissipative and conservative interaction, respectively (at least for $\phi = \pi/2$). Conversely, in dynamic force

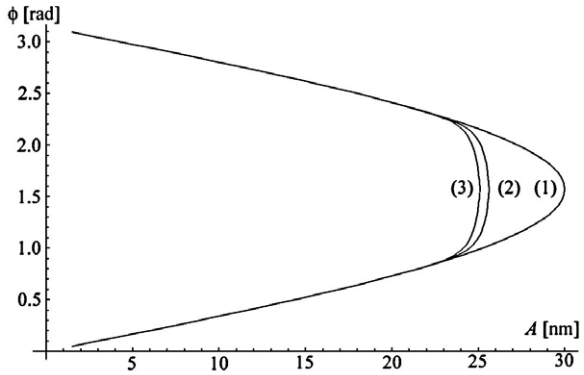

Figure 4. Phase plots for $\Gamma = 10^{-4}$ kg s^{-1} and different separations ((1) $L = A_0 + 150\sigma$; (2) $L = A_0 + \sigma$; (3) $L = A_0$).

spectroscopy experiments, the separation is swept and variations in both amplitude and frequency are recorded (case (iii)). Therefore, in case (i) instabilities would show up in scan images as 'jumps' in L (i.e. in the topography) and/or f while the distance stabilization feedback loop (maintaining constant A) is active, whereas in case (ii) jumps in L and/or A would occur in images while f is stabilized by the feedback loop. Finally, in case (iii), jumps in f and/or A would occur on the approach/withdrawal curves obtained by sweeping L.

4.1. Case (i) (stabilized amplitude)

Here, A is held constant by the distance stabilization feedback loop, A_d is held constant in the CE mode by the self-oscillator AGC feedback circuit, and ϕ is constant by virtue of the SO method, while f and L are allowed to vary. As stated above, while laterally scanning the surface, changes in the interaction potential may induce frequency shift and topography (L) adjustments. Since ϕ is constant, equation (1) implies that $Q_\mathrm{eff}(A_\mathrm{set}, L) = A_\mathrm{set}/A_\mathrm{d} \sin\phi =$ constant. Since $A = A_\mathrm{set}$ and A_d are constant, L will be adjusted such that $A_\mathrm{d} \sin\phi/A_\mathrm{set} = (1/Q + \pi P_\mathrm{surf}/kA_\mathrm{set}^2)$. For instance, $\Gamma = 0$ requires that $A_\mathrm{set}/A_\mathrm{d} \sin\phi = Q$. Thus, as already known, amplitude variation is not possible with no additional tip/sample dissipation, hence amplitude stabilization would not be possible in that case.

Instability may occur if there exist two or more states with equal A and ϕ, at different L and/or f. To analyse this issue, it is necessary to calculate the isophase curves, trace an $A = A_\mathrm{set}$ line, and look for multiple intersections with the isophase curve. This is necessary because phase does not depend on A in the same way for any L as in the purely conservative case; now, different interactions (which depend on L) lead to a change in the phase/amplitude relationship through the distance dependence of the term Q_eff. This is evident from figure 4, where phase versus amplitude plots for a given friction coefficient and different separations are compared. As can be easily realized graphically, however, in this case such multiple intersections are not possible.

4.2. Case (ii) (stabilized frequency)

Now, f is held constant by the distance stabilization feedback loop, A_d is held constant by the AGC, and ϕ is constant, while A and L are allowed to vary. While laterally scanning the sample, changes in the interaction potential may here induce both amplitude and topography adjustments. From equations (1), (3) and (7), in the case of small frequency shift to simplify calculations, we have:

$$f(A, L) = f_\mathrm{r}(A, L) - \frac{f_0 A_\mathrm{d} \cos\phi}{2A}. \tag{9}$$

Since $f(A, L) = f_\mathrm{set}$ and A_d are constant, both the resonance frequency shift, induced by conservative potential changes, as well as the amplitude, determined by the dissipative interaction, contribute to the adjustment of L in order to keep the oscillation frequency constant. Only for $\phi = \pi/2$, the tip traces surface profiles that only depend on conservative potential.

In this case, a condition necessary for instability is the existence of two or more states with equal f and ϕ, at different L and/or A. Now, we must trace a $f = f_\mathrm{set}$ line and look for multiple intersections with the isophase curve. A check of multiple solutions is analytically more difficult in this case, since there are two variables to take into account, namely L and A. However, by our choice of the model dissipative force of equation (7), equation (1) can be inverted, thus providing an explicit $L(A)$; therefore, isophase curves can readily be carried out. Here we show examples of isophase curves with one to three intersections with a given frequency f_set (figure 3). A further requirement for the occurrence of instability between two states in constant frequency-shift mode is that $\mathrm{d}f/\mathrm{d}L$ has the same sign, so that distance stabilization can be realized for both states. For instance, if we stabilize in the 'repulsive mode' (i.e. $\mathrm{d}f/\mathrm{d}L < 0$), an instability can occur for a different state provided that $\mathrm{d}f/\mathrm{d}L < 0$ for a such state. The switching between the two states is not spontaneous, but it could be induced by a fluctuation in the system if the states are close enough to each other, i.e. if the separation difference between them is not too big compared to the typical system fluctuations.

In the case of three intersections, we show that there exist two states with the same sign of $\mathrm{d}f/\mathrm{d}L$, thereby switching between them is possible during DFM imaging. In particular, triple intersection exists for a phase $\phi < \phi_\mathrm{c}$, where ϕ_c depends on the potential and measurement parameters, as shown later on. Figure 3 shows some possible cases, for a given value of friction coefficient chosen for best illustration ($\Gamma = 10^{-4}$ kg s^{-1}). The resonance curve at large separation 'contains' all phases and is plotted to show all possible 'starting points' of the isophase curves. In contrast, each plotted isophase curve describes the behaviour of the system at all possible separations and a single operation phase. The intersection of the isophase curves with a generic resonance curve at separation L describes the oscillation state of the system at such a separation and phase. We note the non-monotonic shape of the isophase curves, considered as a function $f(A)$, at $\phi < \phi_\mathrm{c}$, intercepting the $f =$ constant line in three points (figure 3(b)). Note that the instability may occur between a state with higher amplitude and attractive interaction (large z_c), but where dissipation is already large enough to provide an inversion of $\mathrm{d}f/\mathrm{d}L$, and a state with lower amplitude (smaller z_c) where the interaction is repulsive. Clearly, the DFM spatial resolution achieved in the attractive state will be much lower, due to the higher z_c, although such an

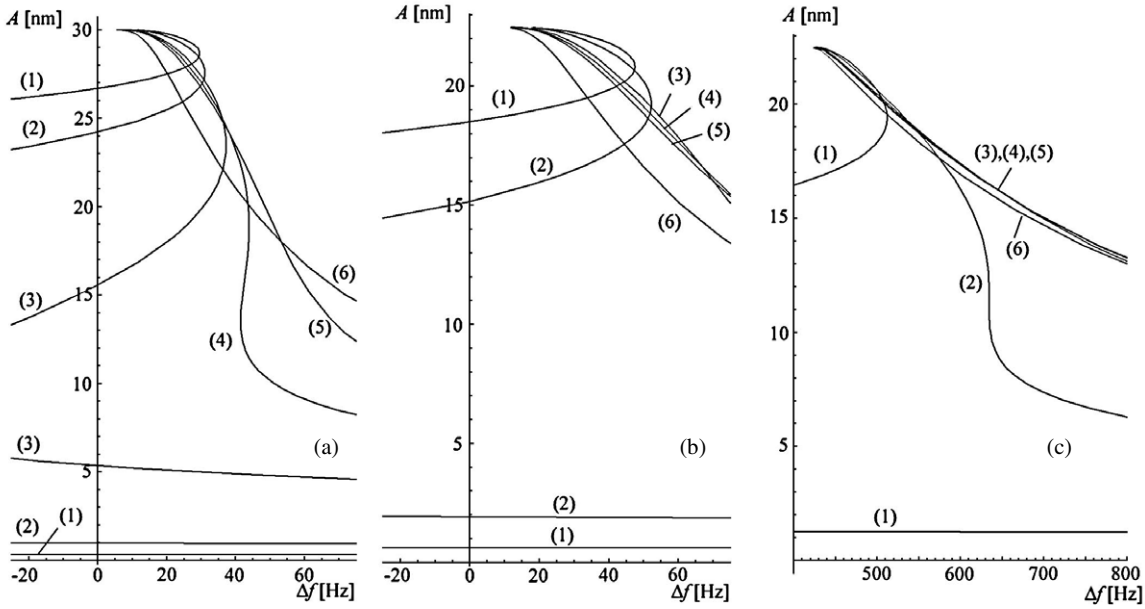

Figure 5. (a) Isophase curves at $\phi_{\rm set} = \pi/2$ for different dissipation coefficients: Γ = (1) 6×10^{-5}, (2) 10^{-4}, (3) 2×10^{-4}, (4) 2.5×10^{-4}, (5) 3×10^{-4}, and (6) 10^{-3} kg s^{-1}. (b) Contribution of the resonant frequency to the isophase curves at $\phi_{\rm set} = 1.4608\pi/2$. (c) Isophase curves at $\phi_{\rm set} = 1.4608\pi/2$.

attractive state may be confused with a repulsive one because of its derivative $\mathrm{d}f/\mathrm{d}L$ being negative as well. Therefore, this instability is similar in many aspects to the typical instability found in tapping mode, with the difference that, instead of a phase jump (with a stabilized amplitude) and switching between an attractive and a repulsive state, here we have an amplitude jump (with a stabilized frequency). Scanning instabilities ('artefacts') in tapping mode were documented for instance in [27], while the effect predicted here for the CE-SO mode is still awaiting experimental verification.

Let us now determine the conditions for the existence of this instability and the value of the critical phase $\phi_{\rm c}$. We look for stationary points of the derivative $(\mathrm{d}f/\mathrm{d}A)_{\phi=\rm const}$ in order to identify local extremal points of the isophase curve. If $L(A)_{\phi=\rm const}$ is a monotonic function, each extremal point of $f(A)_{\phi=\rm const}$ corresponds to one and only one extremal point of $f(L)_{\phi=\rm const}$, which is the relevant function for investigating instability in topography (L) stabilization.

Since $\phi = \phi_{\rm set}$ is a constant, the stationary points of $f(A, L)$ (equation (9)) correspond to the solutions of the equation:

$$\left(\frac{\mathrm{d}f(A,L)}{\mathrm{d}A}\right)_{\phi} = \left(\frac{\mathrm{d}f_{\rm r}(A,L)}{\mathrm{d}A}\right)_{\phi} + \frac{f_0 A_{\rm d}\cos\phi_{\rm set}}{2A^2} = 0. \quad (10)$$

Let us now evaluate $(\mathrm{d}f_{\rm r}(A,L)/\mathrm{d}A)_{\phi=\rm const}$ with our model potentials. By expressing equation (5) as $f_{\rm r}(A,L) = f_0[-M_2 Z_2(A,\phi) + M_6 Z_6(A,\phi)]$, where $M_2 = -C_2 I(2)/(2^{1/2}\pi k)$, $M_6 = C_6 I(6)/(2^{1/2}\pi k)$, $Z_2(A,\phi) = (L(A) - A)^{-3/2}A^{-3/2}$, and $Z_6(A,\phi) = (L(A) - A)^{-11/2}A^{-3/2}$, we have:

$$\left(\frac{\mathrm{d}f_{\rm r}(A,L(A,\phi))}{\mathrm{d}A}\right)_{\phi} = f_0\left[-M_2\left(\frac{\mathrm{d}Z_2(A,\phi)}{\mathrm{d}A}\right)_{\phi} + M_6\left(\frac{\mathrm{d}Z_6(A,\phi)}{\mathrm{d}A}\right)_{\phi}\right]. \quad (11)$$

From equations (7) and (9), we get explicit forms for $L(A)$ and its derivative:

$$L(A,\phi) = A - \sigma\left[\tfrac{1}{2}\ln A - \ln\left(1.6\pi\sigma^{3/2} f_0 \Gamma Q/k\right) + \ln\left(A_0\sin\phi - A\right)\right] \quad (12)$$

$$\left(\frac{\mathrm{d}L}{\mathrm{d}A}\right)_{\phi} = 1 - \sigma\left[\frac{1}{2A} - \frac{1}{A_0\sin\phi - A}\right]. \quad (13)$$

Using such expressions, both $f(A, L(A,\phi))$ and $(\mathrm{d}f(A, L(A,\phi))/\mathrm{d}A)_{\phi=\rm const}$ can be calculated, allowing analysis of the general features of the isophase curves related to equation (9). To illustrate such features, in figure 5(a) isophase curves at different dissipation coefficients are plotted for $\phi_{\rm set} = \pi/2$. At the smaller dissipation values, the isophase curve is characterized by two extremal points: a local maximum at higher amplitudes, and a local minimum at lower amplitudes. By increasing the dissipation coefficient, such extremals disappear and the isophase curve becomes monotonic.

At $\phi_{\rm set} = \pi/2$ we have that $f(A,L)$ is always equal to the resonant frequency $f_{\rm r}(A,L)$. For a phase different from $\pi/2$, such a term is added by a term that is divergent for small amplitudes, $\Delta f_{\rm r}(A,\phi_{\rm set}) = -f_0 A_{\rm d}\cos\phi_{\rm set}/2A$, the sign of which depends on $\phi_{\rm set}$ being greater or smaller than $\pi/2$. Let us consider a phase value different from $\pi/2$ in order to analyse the effect of such a term. For instance, we have chosen a value of $\phi_{\rm set}$ that provides an inflection point in our isophase curves calculated for $\Gamma = 10^{-4}$ kg s^{-1}, as shown later ($\phi_{\rm set} = 1.4608\pi/2$, or about 131°). The trend of the resonant frequency $f_{\rm r}(A,L)$ is shown in figure 5(b). It is very similar to that at $\phi_{\rm set} = \pi/2$, except that the free oscillation frequency is different from f_0 and that the trend becomes monotonic for a lower dissipation coefficient than in figure 5(a). Figure 5(c) shows $f(A,L)$, that is, including the effect of $\Delta f_{\rm r}$, which further lowers such a limiting dissipation

coefficient. For $\Gamma = 10^{-4}$ kg s^{-1}, we indeed have two extremal points in both figures 5(a) and (b), while in figure 5(c) an inflection point is present. For $\Gamma = 2 \times 10^{-4}$ kg s^{-1}, instead, the isophase curve in figure 5(b) already becomes monotonic, even without the further contribution of Δf_r.

Conversely, at a fixed dissipation coefficient, a critical value of phase ϕ_c exists, below which the isophase curve is characterized by two local extremal points, therefore allowing for instability effects when operating in the constant-frequency shift mode. Such a critical value can be determined by solution of equation (10), as in the following example. Let us evaluate graphically the solutions of equation (10) with $(\mathrm{d}f_r(A, L)/\mathrm{d}A)_{\phi=\mathrm{const}}$ given by equation (11), and in the case of $\Gamma = 10^{-4}$ kg s^{-1}. Figure 6 shows the derivative $(\mathrm{d}f(A, L)/\mathrm{d}A)_{\phi=\mathrm{const}}$ plotted for the same values of phase used for the isophase curves of figure 3. Hence, its zeros represent stationary points of the isophase curves. For $\phi = 1.52\pi/2$ (curve (8)), no intersection exists, therefore the corresponding isophase curve must be monotonic. This holds for all phase values greater than the critical phase value ϕ_c, where the derivative is a tangent to the abscissa axis (curve (7)), meaning that the corresponding isophase curve is still monotonic but has an inflection point. For $\phi < \phi_c$ (curves (1)–(6)), two zeros exist. Therefore, the isophase curve must have two local extermal points with opposite curvature, i.e. one local minimum and one local maximum. Such extremal points define three distinct regions with alternate sign of the derivative $(\mathrm{d}f/\mathrm{d}A)_{\phi=\mathrm{const}}$ and consequently of $(\mathrm{d}f/\mathrm{d}L)_{\phi=\mathrm{const}}$. However, for phase values far from ϕ_c (that is, $1.4608\pi/2$ in this case), the first minimum (at small amplitude) corresponds to amplitude values too small to be achieved in high-amplitude DFM, and furthermore the condition $A \gg \sigma$ would not be fulfilled in that region. For phase values closer to ϕ_c, though, the amplitude of such a state can be high enough to represent an actual state of the system. By having a closer look at the solutions of equation (10) (figure 6) we note that, for instance at $\phi = 1.43\pi/2$ (curve (4)), the minimum is located at $A \approx 8.5$ nm, while the maximum is at $A \approx 14.5$ nm. By looking at the corresponding isophase curve (figure 3(b), curve (4)), as an example, at $\Delta f = 500$ Hz three intersections with the isophase curve exist at amplitudes $A_1 \approx 6.5$ nm, $A_2 \approx 12$ nm, and $A_3 \approx 19.5$ nm. Amplitudes A_1 and A_3 present the same sign of $(\mathrm{d}f/\mathrm{d}A)_{\phi=\mathrm{const}} < 0$, and A_1 is reasonably high compared to σ. However, such states still seem too far apart to lead to instabilities in actual experiments. For higher dissipation coefficient values, the two states have the tendency to become closer, as is visible, for instance, in figure 5(a). Furthermore, strong fluctuations could also be induced by DFM surface scanning, due to spatial variations of local potentials. Such variations may induce instabilities much more efficiently than just system noise. Therefore, experimental studies are still needed to evaluate the role of such effects in the actual DFM performance in CE-SO mode. As for the extension to vacuum operation, we note that, in such a system, the role of surface dissipation becomes increasingly important, since the relative contribution to Q_{eff} of surface dissipation increases for higher lever-Q, as seen by equation (8). Therefore, since the appearance of instability is essentially related to the onset of surface dissipation in the system, the effect is expected to be present and even enhanced in vacuum systems. Quantitative analysis and comparison to available experimental data will be the subject of further studies.

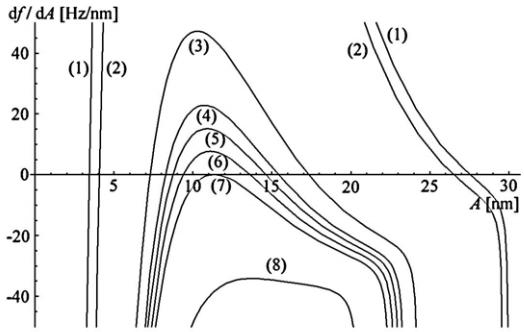

Figure 6. Plots of the left-hand term of equation (10) in the same case and for the same phase values of figure 3.

In the example of figure 3, the critical phase is higher than $\pi/2$, which is the typical working point of SO experiments. Therefore, such experiments would be subjected to this kind of instability effect if the interaction forces were similar to those used for our calculations (which have been chosen to fit the actual experiment of [16]) and the dissipation coefficient was of the order of 10^{-4} kg s^{-1}. Already, for $\Gamma = 10^{-3}$ kg s^{-1} though, the critical phase becomes smaller than $\pi/2$ (namely, $0.926\,05\pi/2$). Then, the usual working point at phase $\pi/2$ may be subjected to instabilities or not, depending on the magnitude of the surface dissipation.

4.3. Case (iii) (approach curves)

Now, L is to be considered a constant, and there is no distance stabilization feedback active. In practice, L is swept slowly to obtain the approach curve, A_d is held constant by the AGC, and ϕ is a constant, while f and A are allowed to vary.

During the approach, L is decreased; this means that z_c (which is related to the amount of interaction) can decrease or increase, depending on A; indeed, the set phase can be met, since A is allowed to vary. Let us describe the behaviour of A and Δf during the performance of an approach curve with the aid of figure 7. The behaviour of A versus L is shown in figure 7(a) as it would appear in actual experiments, for $\phi = \pi/2 < \phi_c$ and $1.5\pi/2 > \phi_c$ for $\Gamma = 10^{-4}$ kg s^{-1}. As already shown in figure 5 of [16], the trend of A versus the closest approach z_c has a turnaround point (figure 7(b)), hence a minimum approach distance is reached while decreasing the separation L and consequently A. The dissipated energy per cycle, $E_{\mathrm{diss}} = P_{\mathrm{surf}}/f$, is also plotted in figure 7(b) (curve (3)). E_{diss} increases until $E_0/4$, a quarter of the free lever energy, at $A = A_0/2$, then decreases again while L decreases. For $A_0/2 > A > A_0/3$, E_{diss} decreases, although z_c is still decreasing. This is due to the competition between the increased dissipation stemming from the closer range and the speed reduction due to the amplitude decrease, which reduces the viscous damping effect. Minimum z_c is reached at $A = A_0/3$ for the chosen potentials. In general, the amplitude of the minimum closest-approach z_c^{min} can be obtained analytically when the dependence of E_{diss} on A and z_c can be factorized, and when the explicit expression of $z_c(A, E_{\mathrm{diss}})$ can be carried

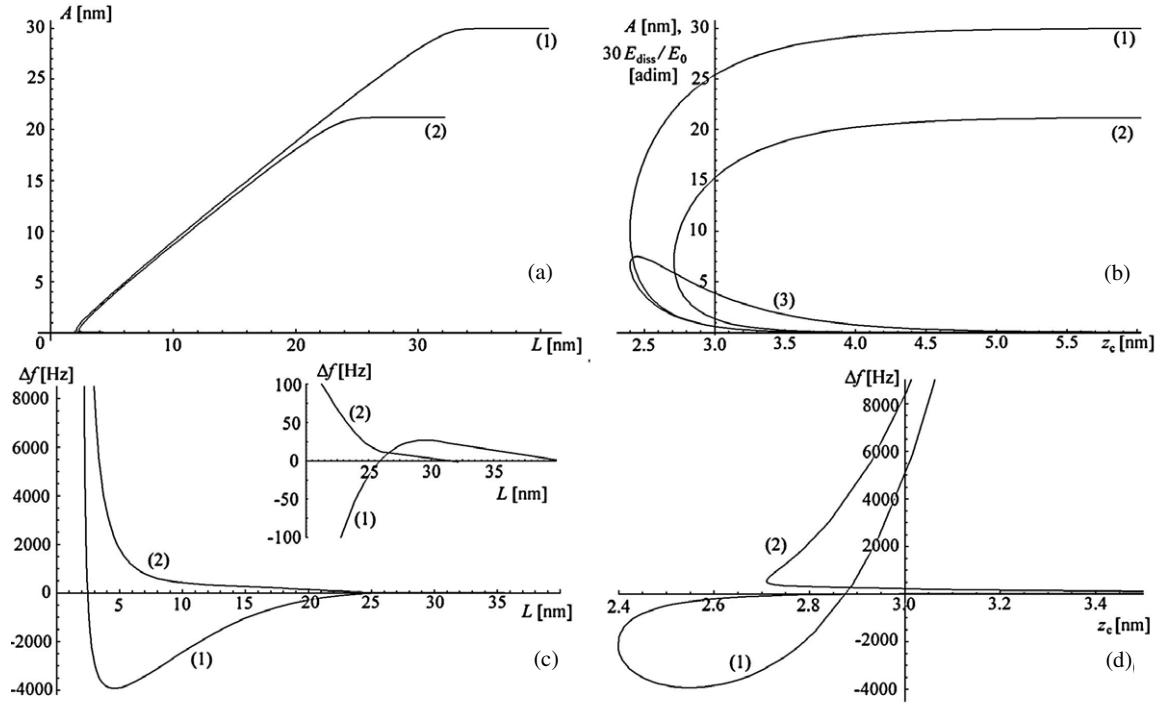

Figure 7. Approach curves for the case $\Gamma = 10^{-4}$ kg s^{-1}. (a) $A(L)$ at (1) $\phi = \pi/2 < \phi_c$ and (2) $\phi = 1.5\pi/2 > \phi_c$; (b) $A(z_c)$ (at the same phase values) and E_{diss} (curve (3), in units of $30E_0$); (c) $\Delta f(L)$—the inset shows the behaviour at large amplitude; (d) $\Delta f(z_c)$.

out; z_c^{min} is found by calculating the stationary point of such a function, by replacing E_{diss} with the expression $E_0 A/A_0(1 - A/A_0)$ [16]. It can be shown that the result $A(z_c^{min}) = A_0/3$ is obtained whenever the dependence on A of E_{diss} is of the form $A^{1/2}$, and is not influenced by the form of its dependence on z_c.

A further decrease in L is accompanied by A decreasing faster than L, so that z_c increases and E_{diss} decreases. Thus, for $A < A_0/3$, the probe/sample interaction weakens as the cantilever base moves closer to the surface; additionally, the maximum E_{diss} is $E_0/4$ at $A = A_0/2$. The frequency shift (figure 7(c)) is monotonic for $\phi > \phi_c$, while for $\phi < \phi_c$ the local extremals in the frequency shift appear. The inset of figure 7(c) shows the expanded view of the frequency shift curves at larger separation, evidencing the local maximum for the curve at $\phi < \phi_c$. The frequency shift is initially increased due to dissipation, afterwards it is decreased due to the attractive force, and finally increased again due to repulsion. Note that, since the function $A(L)$ is monotonic and almost linear (as is visible in figure 7(a)), the frequency shift curves $f(L)$ are qualitatively similar to the isophase curves $f(A)$. In figure 7(d), the same curves are plotted versus z_c. Note the curious 'looping' of the frequency shift at $\phi < \phi_c$.

For the analysis of instability in the approach curves, since L is to be considered fixed, we must deal with a single resonance curve. To identify jumps in either A or f, we should have points on the resonance curve with different values of A or f at a definite ϕ and as we have clearly demonstrated, this is not permitted in the SO method. Therefore the frequency shift curves of figure 7(c) (as well as the isophase curves previously analysed) are followed faithfully during the approach and withdrawal of the cantilever base to the surface, and no instability effects are anticipated.

5. Discussion

Instabilities in approach curves, similar to those found in the tapping mode, seem not to be possible with the SO method, unless admitting that the interaction potential can be modified by the tip approach itself. This corresponds, for instance, to the assumption of hysteretic potentials used to obtain jumps in frequency shift versus separation curves by numerical simulations [12]. Other models, however, could be able to reproduce the experimental evidence of [9, 10]. A 'plastic' deformation of the surface sites, in which the tip interaction helps to overcome some energy barrier to change the surface structure permanently, could also explain the data. The comparison between approach and withdrawal frequency shift curves could indicate whether a plastic deformation concerning the sample surface structure occurs, or if an intermittent formation/breaking of a bound state between tip and sample, as conjectured in [10], takes place. If the withdrawal curve (the same as the approach curve, but obtained while increasing L) was identical to the approach curve, this would support the intermittent bond formation and breaking. On the contrary, if the withdrawal curve differed substantially from the approach curve, for instance showing no discontinuity in the frequency shift, then a permanent change in the surface atom position induced by the tip would be supported. Indeed, DFM in the CE-SO mode has been used to achieve surface nanostructuring at the atomic level [28], supporting the possibility of such a phenomenon. Recent *ab initio* simulations [11] succeeded in reproducing frequency shift jumps, though for a different system than in [10] (Si/InAs instead of Si/Si), thus supporting the possibility of periodic bond formation and breaking, which corresponds to the case of a hysteretic potential. Such a

potential would imply energy dissipation, equivalent to the area of the hysteresis loop in the force–separation plot. Recent experiments support such a velocity-independent dissipation mechanism as the dominant mechanism in DFM, with respect to the customarily assumed viscous damping, at least for a Si/graphite system [29]. Instead, in the case of a single bonding event, no such velocity-independent dissipation should be observed. Therefore, it should be possible to discriminate between the two cases by observing deviations of the amplitude versus separation curve from the trend typical of a non-hysteretic potential (figures 7(a) and (b)). Simultaneous acquisition of frequency and amplitude versus separation curves in CE-SO mode and reiterated measurements on the same atomic site, in both approach and withdrawal directions, would result in useful elements for a correct understanding of the atomic interaction mechanisms, as probed by dynamic force spectroscopy.

6. Conclusion

The stability of the constant-excitation amplitude mode of the self-oscillator method used in dynamic force microscopy was discussed. The analysis was made by looking for multiple oscillation states compatible with phase locking occurring in such a method. Improved stability is confirmed, in comparison with the conventional constant-frequency (tapping-mode) DFM, and in accord with experimental observations. In particular, no instability is anticipated for both constant-dissipation mode imaging (i.e. distance stabilization with constant A) and spectroscopic mode (the acquisition of approach curves). Unstable behaviour is anticipated, for a set phase lower than a critical phase value ϕ_c and in a limited frequency shift regime, for constant-frequency shift imaging in the constant-excitation amplitude mode. The high stability of the SO method indicates that, within the first-order approximated analysis carried out here, jumps in frequency shift recorded in dynamic force spectroscopy experiments are unlikely to be ascribed to instrumental effects, but must necessarily be due to changes in the tip/sample interaction potential (intermittent bond formation and breaking, or permanent surface changes) due to the tip approach to the surface.

Acknowledgments

I wish to thank Alan Gallagher (JILA, Boulder) for many stimulating discussions, for his continuous support, and for his precious help during the preparation of the manuscript. I also thank the reviewers for their useful comments and suggestions.

References

[1] Albrecht T R, Grütter P, Horne D and Rugar D 1991 *J. Appl. Phys.* **69** 668
[2] Martin Y, Williams C C and Wickramasinghe H K 1987 *J. Appl. Phys.* **61** 4723
[3] Zhong Q, Inniss D, Kjoller K and Elings V B 1993 *Surf. Sci. Lett.* **290** 688
[4] Hölscher H, Gotsmann B, Allers W, Schwarz U D, Fuchs H and Wiesendanger R 2001 *Phys. Rev.* B **64** 075402
[5] Hölscher H, Gotsmann B and Schirmeisen A 2003 *Phys. Rev.* B **68** 153401
[6] Kühle A, Sørensen A H and Bohr J 1997 *J. Appl. Phys.* **81** 6562
[7] Gauthier M and Tsukada M 2000 *Phys. Rev. Lett.* **85** 5348
[8] Ueyama H, Sugawara Y and Morita S 1998 *Appl. Phys.* A **66** (Suppl.) 295
[9] Uchihashi T, Sugawara Y, Tsukamoto T, Ohta M, Morita S and Suzuki M 1997 *Phys. Rev.* B **56** 9834
[10] Morita S, Sugawara Y, Yokohama K and Uchihashi T 2000 *Nanotechnology* **11** 120
[11] Caciuc V, Holscher H, Blugel S and Fuchs H 2005 *Nanotechnology* **16** S59
[12] Gotsmann B and Fuchs H 2002 *Appl. Surf. Sci.* **188** 355
[13] Schirmeisen A, Holscher H, Anczykowski B, Weiner D, Schafer M M and Fuchs H 2005 *Nanotechnology* **16** S13
[14] Magonov S N, Elings V and Whangbo M-H 1997 *Surf. Sci.* **375** L385
[15] Cleveland J P, Anczykowski B, Schmid A E and Elings V B 1998 *Appl. Phys. Lett.* **72** 2613
[16] Protasenko V V, Labardi M and Gallagher A 2004 *Phys. Rev.* B **70** 245414
[17] Stark M, Stark R W, Heckl W M and Guckenberger R 2000 *Appl. Phys. Lett.* **77** 3293
[18] Giessibl F J 1997 *Phys. Rev.* B **56** 16010
[19] Dürig U 1999 *Appl. Phys. Lett.* **75** 443
[20] Gotsmann B, Seidel C, Anczykowski B and Fuchs H 1999 *Phys. Rev.* B **60** 11051
[21] Bogart T F Jr 1993 *Electronic Devices and Circuits* 3rd edn (New York: Macmillan)
[22] Gauthier M, Sasaki N and Tsukada M 2001 *Phys. Rev.* B **64** 085409
[23] Gauthier M, Pérez R, Arai T, Tomitori M and Tsukada M 2002 *Phys. Rev. Lett.* **89** 146104
[24] Couturier G, Boisgard R, Nony L and Aimé J P 2003 *Rev. Sci. Instrum.* **74** 2726
[25] Holscher H, Gotsmann B, Allers W, Schwarz U D, Fuchs H and Wiesendanger R 2002 *Phys. Rev. Lett.* **88** 019601
[26] Jarvis S P, Yamada H, Kobayashi K, Toda A and Tokumoto H 2000 *Appl. Surf. Sci.* **157** 314
Protasenko V V, Gallagher A and Nesbitt D J 2002 *Proc. SPIE—Int. Soc. Opt. Eng.* **4809** 255
[27] Kühle A, Sørensen A H, Zandbergen J B and Bohr J 1998 *Appl. Phys.* A **66** (Suppl.) 329
[28] Oyabu N, Custance O, Yi I, Sugawara Y and Morita S 2003 *Phys. Rev. Lett.* **90** 176102
[29] Schirmeisen A and Holscher H 2005 *Phys. Rev.* B **72** 045431